

OFFICE OF NAVAL RESEARCH  
Research Contract N00014-87-K-0014  
R&T Code 413a001

Technical Report No. 22

SYMMETRY BREAKING AND ELECTRONIC MIXING OF CRYSTAL STATES  
BY THE SCANNING TUNNELING MICROSCOPE

by

R. Stanley Williams, David Farrelly,  
Elliott A. Eklund and Eric J. Snyder

AD-A210 030

Submitted  
to  
*Nature*

SDTIC  
ELECTE  
JUN 22 1989  
CH

University of California, Los Angeles  
Department of Chemistry & Biochemistry and Solid State Science Center  
Los Angeles, CA 90024-1569

July 1, 1989

Reproduction in whole or part is permitted for any purpose of the United States Government.

This document has been approved for public release and sale;  
its distribution is unlimited

89 6 21 020

## REPORT DOCUMENTATION PAGE

1a REPORT SECURITY CLASSIFICATION UNCLASSIFIED			1b RESTRICTIVE MARKINGS N/A		
2a SECURITY CLASSIFICATION AUTHORITY N/A			3 DISTRIBUTION / AVAILABILITY OF REPORT Approved for public release; distribution unlimited		
2b DECLASSIFICATION / DOWNGRADING SCHEDULE N/A					
4 PERFORMING ORGANIZATION REPORT NUMBER(S) N/A			5 MONITORING ORGANIZATION REPORT NUMBER(S)		
6a NAME OF PERFORMING ORGANIZATION The Regents of the University of California		6b OFFICE SYMBOL (if applicable)	7a NAME OF MONITORING ORGANIZATION 1) ONR Pasadena - Administrative 2) ONR Alexandria - Technical		
6c ADDRESS (City, State, and ZIP Code) Office of Contracts & Grants Administration U C L A, 405 Hilgard Avenue Los Angeles, CA 90024			7b ADDRESS (City, State, and ZIP Code) 1) 1030 E. Green Street, Pasadena, CA 91106 2) 800 N. Quincy St., Arlington, VA 22217-5000		
8a NAME OF FUNDING / SPONSORING ORGANIZATION Office of Naval Research		8b OFFICE SYMBOL (if applicable) ONR	9 PROCUREMENT INSTRUMENT IDENTIFICATION NUMBER N00014-87-K-0014		
8c ADDRESS (City, State, and ZIP Code) 800 N. Quincy Street, 614A:DHP Arlington, VA 22217-5000			10 SOURCE OF FUNDING NUMBERS		
			PROGRAM ELEMENT NO.	PROJECT NO.	TASK NO.
					WORK UNIT ACCESSION NO.
11 TITLE (Include Security Classification) UNCLASSIFIED: Symmetry breaking and electron mixing of crystal states by the Scanning Tunneling Microscope					
12 PERSONAL AUTHOR(S) R. Stanley Williams, David Farrelly, Elliott A. Fklund and Eric J. Snyder					
13a TYPE OF REPORT Tech Rept # 22		13b TIME COVERED FROM 1988 TO 1989		14 DATE OF REPORT (Year, Month, Day) 15 June 1989	15 PAGE COUNT 20
16 SUPPLEMENTARY NOTATION					
17. COSATI CODES			18 SUBJECT TERMS (Continue on reverse if necessary and identify by block number)		
FIELD	GROUP	SUB-GROUP	→ surface structure probe - distortion of Fermi surface - STM topographs - degeneracy of k states - tunneling tip.		
19. ABSTRACT (Continue on reverse if necessary and identify by block number)					
<p>The Scanning Tunneling Microscope (STM) is usually assumed to provide a non-intrusive probe of the surface structure of materials. Experimental and theoretical studies of the (0001) surface of graphite have demonstrated that the crystal states can be influenced by the electric field of the tunneling tip. Therefore, the resulting STM topographs may not arise from the ground electronic state of the system. An ultra-low-noise STM has been used to show that the graphite surface reproducibly gives rise to two <i>different</i> rotational symmetric images as a function of the field supplied by the STM. A theoretical interpretation of all the commonly observed graphite STM images is given in terms of the degree to which the Fermi surface is altered by the finite range and non-uniformity of the applied electric field and by any asymmetries of the tip. Recognition of the coupling of the STM tip with the sample has far-reaching implications for the use of this technique in determining the atomic and electronic structures of surfaces.</p>					
20 DISTRIBUTION / AVAILABILITY OF ABSTRACT <input checked="" type="checkbox"/> UNCLASSIFIED/UNLIMITED <input type="checkbox"/> SAME AS RPT <input type="checkbox"/> DTIC USERS			21 ABSTRACT SECURITY CLASSIFICATION UNCLASSIFIED		
22a NAME OF RESPONSIBLE INDIVIDUAL R. Stanley Williams			22b TELEPHONE (Include Area Code) (213) 825-8818		22c OFFICE SYMBOL UCLA

# Symmetry Breaking and Electronic Mixing of Crystal States by the Scanning Tunneling Microscope

R. Stanley Williams, David Farrelly, Elliott A. Eklund, and Eric J. Snyder

Department of Chemistry and Biochemistry

University of California

Los Angeles, CA 90024-1569

USA

**Abstract:** The Scanning Tunneling Microscope (STM) is usually assumed to provide a non-intrusive probe of the surface structure of materials. Experimental and theoretical studies of the (0001) surface of graphite have demonstrated that the crystal states can be influenced by the electric field of the tunneling tip. Therefore, the resulting STM topographs may not arise from the ground electronic state of the system. An ultra-low noise STM has been used to show that the graphite surface reproducibly gives rise to two *different* rotationally symmetric images as a function of the field supplied by the STM. A theoretical interpretation of all of the commonly observed graphite STM images is given in terms of the degree to which the Fermi surface is altered by the finite range and non-uniformity of the applied electric field and by any asymmetries of the tip. Recognition of the coupling of the STM tip with the sample has far-reaching implications for the use of this technique in determining the atomic and electronic structures of surfaces.

Beautiful topographs of crystal surfaces obtained with the Scanning Tunneling Microscope (STM) are appearing ever more frequently in the scientific and popular literature. With the availability of relatively inexpensive commercial instruments, scientists from a wide range of disciplines are able to examine their samples with the STM, and in some cases observe features with *atomic-scale* resolution. In order to test out and tune up new instruments, most researchers examine a freshly cleaved surface of highly-oriented pyrolytic graphite (HOPG). This surface readily provides tunneling signals with large variations in tunneling current as a function of tip position for constant bias (constant height mode), resulting in striking atomic scale images of well characterized symmetry and geometry. Problematically, however, the same section of the graphite surface, scanned using the same tip in the same experiment, gives rise to several different, but characteristic, images depending on the particular experimental conditions (see Figs. 1 and 2).

The six images in Figs. 1 and 2 were collected in constant height mode with an STM built at UCLA. This instrument was constructed to have especially low thermal drift, mechanical instability, and electrical noise characteristics, so that current topographs could be displayed with a minimum of image processing. The images presented here were subjected only to a nine-point smoothing procedure (i.e., each data point was averaged with weighted contributions from its nearest and next-nearest neighbors) in order to damp the high frequency ripple in the scan lines. Figs. 1a, 1b, and 1c (2a, 2b, and 2c) represent topographs obtained with the tunneling tip biased at +22, +25, and +39 mV (-22, -25, and -39 mV) respectively with respect to the sample. The average current for all the scans was 0.9 nA, and the images display the variation (typically less than  $\pm 0.1$  nA) of the current about that average as a function of lateral tip position over the graphite surface. These topographs illustrate some general trends observed in an experiment in which nearly 100 images were obtained. At low applied fields, the topographs collected with the same magnitude of the potential but different polarity have essentially the same features, although the size of the corrugations may be different. As the strength of the applied field is increased,

either by increasing the potential or decreasing the sample to tip distance, the image changes from an asymmetric honeycomb, such as that of Fig. 1a, to a close packed array, such as in Fig. 1b, and then back to the honeycomb, as in Fig. 1c. These types of changes were reversible and highly reproducible, which is evidence that they are not caused by changes in the geometry of the tip. This trend continues until, at higher fields, the images sometimes become skewed and lose rotational symmetry to form row patterns. If STM is to develop into a routine technique for determining surface structure, one must be able to rationalize all the different images in terms of a specific atomic geometry.

For graphite, in an *ad hoc* fashion, Mizes, Park, and Harrison[1] were able to synthesize many of the commonly observed STM images of HOPG by artificially varying the relative amplitudes of just six Fourier coefficients to match experimental results[2]. They postulated that physical asymmetries of the tip, perhaps arising from a group of atoms acting as a multiple tunneling center, are responsible for modulating the intensity and the phase with which each of the Fourier components contributes to the image. They concluded that it was not possible to determine experimentally which type of image actually corresponded to the 'correct' image of a graphite surface, because of the complications introduced by a multiple-atom tip. This is significant since it implies that STM would not be able to determine the atomic structure of the graphite surface uniquely in the absence of other information.

In STM experiments of graphite, two basic classes of topograph emerge: those images displaying 6- or 3-fold rotational symmetry (the close packed and honeycomb patterns shown in Figs. 1 and 2) fall into one class, and those which do not (the row patterns shown in Ref. 1) fall into the other. Using a simplified model of graphite in which the crystal is treated as a perturbed *monolayer*, it has recently been demonstrated (using a real space analysis), that the rotationally symmetric images can be thought of as being quantal interference patterns between two nearly degenerate wavefunctions lying at the Fermi level, which states are mixed by the perturbation



<input checked="" type="checkbox"/>	
<input type="checkbox"/>	
<input type="checkbox"/>	
Codes	
Dist	Avail and/or Special
A-1	

provided by the STM tip and concomitant electric field[3]. States at the Fermi level ( $E_F$ ) arise almost entirely from the B atoms of graphite (Fig. 3a)[4,5], and the perturbed wavefunctions are constructed from symmetric and anti-symmetric linear combinations of states with  $k$  vectors oriented towards the six corners of the hexagonal two dimensional Brillouin zone (BZ) [3]. A major new experimental result of the present paper, as shown in Figs. 1 and 2, is the demonstration that both types of rotationally symmetric images are robust structures that can reproducibly be obtained as a function of applied field; neither is caused by uncontrollable multi-atom tunneling[1-3]. This insight is possible because of the high stability of the STM, which enables raw data to be examined without arbitrary image processing. However, this result also requires that a consistent theoretical picture be constructed to explain how both the rotationally symmetric and the non-symmetric images arise. The major theoretical result of this paper, building on the simplified model of Ref. 3, is to show that a reciprocal space interpretation of the interaction of the tip (and applied field) with certain crystal  $k$ -states can explain *all* of the observed graphite images, and other important aspects of the STM experiments, such as the similarity of the topographs with respect to changing the bias polarity, the large corrugations observed in the topographs, and the surprising ease with which atomic scale graphite images can be obtained.

The remainder of the paper is organized as follows: first, a simple reciprocal-space model is introduced that can be used to understand the interaction of the graphite surface and the STM tip. The physical origin of the Fourier coefficients that determine the STM topographs is identified and the change in magnitude induced in them by a localized electric field and by tip asymmetry is discussed. The effectiveness and validity of the model are demonstrated by reference to the trends in the STM images of Figs. 1 and 2. Finally, the broader implications of this model to the analysis of STM results are presented.

A topograph obtained with the STM operating in constant height mode can be thought of as being the real-space projection of the states lying at or close to  $E_F$  onto a plane parallel to the

cleavage surface of graphite, denoted  $\rho(r, E_F)$ , which is broadened by an appropriate response function  $b(r)$  characteristic of the tip. (In Tersoff's analysis [10], the constant current STM topograph is considered to be a map of constant-density contours.) The Fourier transform (FT) of an experimental image is given by the well known result,

$$F[\rho(r, E_F) * b(r)] = F[\rho(r, E_F)] \times F[b(r)] \quad , \quad (1)$$

which is to say that the FT of the surface-projected states at  $E_F$  convoluted with the tip response function is equal to the product of the FT of the surface-projected states and the FT of the tip response. A physically reasonable model for the real-space response function  $b(r)$  is a two-dimensional Gaussian, which makes  $F[b(r)]$  a Gaussian also. This assumption simplifies the analysis and provides a great deal of insight. If a blunt tip is represented by a  $b(r)$  with a large full width at half maximum, then  $F[b(r)]$  will be a very narrow function in reciprocal space. Thus,  $F[b(r)]$  will suppress the Fourier coefficients of  $F[\rho(r, E_F)]$  at non-zero wavevector in the product of eq. 1, and the periodic signal in the real-space topograph will be decreased with respect to the small wavevector random noise. By analyzing the Fourier transform of the real space topograph, it may be possible (in principle) to determine  $F[b(r)]$  and  $F[\rho(r, E_F)]$  separately, but first the symmetry and nature of  $F[\rho(r, E_F)]$  must be better understood.

Specifically,  $F[\rho(r, E_F)]$  is the projection of the states at  $E_F$  onto the reciprocal-space plane that has 6-fold rotational symmetry, i.e., the projection of the Fermi surface onto the hexagonal face of the graphite BZ in the extended zone scheme. The band structure and Fermi surface of graphite have been thoroughly characterized [6-9], and a schematic representation of the Fermi surface is shown in Fig. 3b, with its projection onto the hexagonal surface of the first BZ shown in Fig. 4a. The Fermi surface comprises elongated and nearly ellipsoidal structures with their major axes centered on the P lines of the three-dimensional BZ [6]. As Tersoff[10] has noted, the planar projection of the Fermi surface appears as a filled circle at each corner ( $\bar{P}$ ) of the two-

dimensional BZ (this projection is actually trigonally distorted, but that level of detail is not essential for most of the present discussion). This Fermi surface map is now identifiable as the origin for the six Fourier coefficients obtained empirically by Mizes *et al.*, [1] who calculated a Patterson map of the surface electronic states near  $E_F$  by Fourier transforming an STM image with a close-packed array of circular features. Thus, such a close-packed array is the intrinsic image of the graphite surface in the absence of any perturbations of the crystal states, and corresponds to imaging of only the B sites of the graphite surface, since they are the primary contributors to the states at  $E_F$  [4, 5].

This should not be taken to mean that the topographs with 3-fold symmetry observed for graphite are necessarily anomalous or are caused by multiple-atom tips. In fact, STM topographs of graphite which do not exhibit 6-fold symmetry are also legitimate structures requiring theoretical interpretation. All the images are easily explained by consideration of symmetry breaking in the surface plane of the graphite crystal by the STM tip. The mere presence of the tunneling tip is enough to break the translational symmetry parallel to the surface, and thus the components of the wavevector in the plane of the two-dimensional BZ ( $k_x$  and  $k_y$ ) are no longer strictly good quantum numbers. Insight into how the tip affects the Fourier coefficients of  $F[\rho(\mathbf{r}, E_F)]$  can be obtained by considering two limiting cases: the lifting of ground-state degeneracies, i.e., the distortion of the Fermi surface, by a cylindrically symmetric and localized Stark field, and the effect of a tip response function  $b(\mathbf{r})$  that does not have cylindrical symmetry.

The theory outlined here and in Ref. 3 differs from that of Tersoff [10] in that the effect of the tip is explicitly considered; the presence of a local field mixes the ground state wavefunctions to form new states that are actually responsible for producing the STM topograph. Define  $H$  to be the ground-state Hamiltonian for a semi-infinite graphite slab, with  $\psi_{\mathbf{k}}(\mathbf{r})$  and  $\psi_{-\mathbf{k}}(\mathbf{r})$  being eigenfunctions (Bloch functions) of the Hamiltonian with *almost* degenerate

eigenvalues on the Fermi surface (trigonal warping of the Fermi surface lifts the exact degeneracy [8]). Then

$$V(\mathbf{r}) = -ez \mathcal{E}(\mathbf{r}) \quad (2)$$

is the perturbation experienced by electrons near the graphite surface, i.e., it is the energy of an electron in the Stark field generated by the tip. In this example,  $\mathbf{k}$  and  $-\mathbf{k}$  are constrained to lie in the reciprocal-space  $k_x$ - $k_y$  plane ( $k_z$  breaks down as a quantum number near the crystal surface),  $e$  is the electron charge, and  $z$  is the coordinate perpendicular to the plane of the graphite surface.

The electric field  $\mathcal{E}(\mathbf{r})$  is assumed to be non-homogeneous but cylindrically symmetric about the  $z$  direction (an ideal tip), decreasing in strength at the surface plane as a function of radial distance from the axis of symmetry. Because of the small tip-surface distance, the maximum *field* is quite large ( $>10^5$  Vcm $^{-1}$ ), depending both on the applied voltage and tip-surface separation. The matrix elements describing the interaction of the graphite states with the field are then given by [11],

$$V_{\mathbf{k},\mathbf{k}'} = - \int \psi_{\mathbf{k}}^\dagger(\mathbf{r}) ez \mathcal{E}(\mathbf{r}) \psi_{\mathbf{k}'}(\mathbf{r}) d\mathbf{r} . \quad (3)$$

This restricted example is a two-state system involving almost degenerate  $\mathbf{k}$ -states which can be solved exactly to yield the new eigenvalues for the graphite surface in the presence of the tip[12],

$$E_{1,2} = \frac{1}{2} (H_{\mathbf{k},\mathbf{k}} + V_{\mathbf{k},\mathbf{k}} + H_{-\mathbf{k},-\mathbf{k}} + V_{-\mathbf{k},-\mathbf{k}}) \pm \frac{1}{2} \sqrt{(H_{\mathbf{k},\mathbf{k}} + V_{\mathbf{k},\mathbf{k}} - H_{-\mathbf{k},-\mathbf{k}} - V_{-\mathbf{k},-\mathbf{k}})^2 + 4|V_{\mathbf{k},-\mathbf{k}} \times V_{-\mathbf{k},\mathbf{k}}|} \quad (4)$$

For cases in which  $\mathbf{k}$  and  $\mathbf{k}'$  differ, the  $V_{\mathbf{k},\mathbf{k}'}$  matrix element is zero for a uniform field (i.e., a homogeneous field of infinite spatial extent). However, for a non-homogeneous field, (e.g., one that decays from its maximum to zero over a lateral distance comparable to several unit cells) such as that supplied by the STM tip, the integral in eq. 3 will be dominated by the stationary phase or saddle points of the integrand. New states with different wavefunctions that are linear combinations of  $\psi_{\mathbf{k}}(\mathbf{r})$  and  $\psi_{-\mathbf{k}}(\mathbf{r})$  will thus be created (since the ground states with  $+\mathbf{k}$  and  $-\mathbf{k}$  wavevectors are not exactly degenerate essentially any linear combination is possible). Even though the magnitude of the perturbation is small compared to the eigenvalues of the ground-state Hamiltonian ( $H_{\mathbf{k},\mathbf{k}}$  and  $H_{-\mathbf{k},-\mathbf{k}}$ ), the mixing of the states can be very strong as long as the two terms in the square root of eq. 4 are comparable in magnitude. In principle, *all* of the states near the Fermi surface can be coupled by the electric field supplied by the tip, and in order to make an *ab initio* prediction of the STM image for a particular field generated at the tip, the eigenstates of the full Hamiltonian  $H + V$  must be determined. Such a calculation is not practical; one reason being that the field  $\mathcal{E}(\mathbf{r})$  is not well characterized.

The fact that the degeneracy of the plus and minus  $\mathbf{k}$  states can be lifted by the Stark field is one cause of the different intensities observed for the Fourier coefficients of the reciprocal-space STM image. Since one must consider the star of  $\mathbf{k}$ , i.e., all states with equal magnitude of the wavevector for a particular state on the Fermi surface, the Fourier coefficients for graphite

would be expected to alternate in intensity around the two-dimensional BZ, as illustrated in Fig. 4b. This effect was demonstrated explicitly in Ref. 3, where mixing of two wavefunctions constructed from the star of  $k$  produced a real-space topograph with alternating intensities around the rings of a honeycomb lattice. Because of the complex interaction among the large number of degenerate states, the variation in the intensities of the Fourier coefficients should oscillate (i.e., the reciprocal space images will change back and forth between Figs. 4a and 4b) with increasing field strength until the field is increased up to the point at which the Fermi surface is so severely distorted from its ground state form that neither Fig. 4a nor 4b can represent the Fourier coefficients of the perturbed eigenfunctions. This is the type of behavior experimentally observed in the STM images in Figs. 1 and 2, with the 6-fold rotationally symmetric topographs of Figs. 1b and 2b corresponding to the reciprocal-space representation of Fig. 4a, and the remaining topographs, all with essentially 3-fold symmetry, to the FT image of Fig. 4b.

At first, it might seem paradoxical that a cylindrically symmetric perturbation could lower the rotational symmetry of the STM topograph of graphite. However, the unperturbed states at the graphite Fermi surface only appear to have a higher symmetry than the crystal. This is because the B atoms, which by themselves have 6-fold symmetry, are the dominant contributors to states at  $E_F$  [4]. The perturbation due to the tip can strongly mix the states associated with just the B atoms, as shown in Ref. 3, and yield new states with the actual 3-fold rotational symmetry of the graphite lattice; i.e., enhance the trigonal distortion of the Fermi surface by breaking the translational symmetry at the crystal surface. Thus, topographs such as Fig. 1c, which display distinct triangular protrusions with alternating heights arranged on a honeycomb lattice, are intrinsic to a graphite surface in the presence of a localized perturbation[3], and are not the result of tip asymmetries[1].

The STM topographs that are not rotationally symmetric, i.e., the row patterns, are the result of asymmetric tips. This can be understood by considering the effect of an asymmetric

response function in eq. 1. If  $b(\mathbf{r})$  is assumed to be a two-dimensional Gaussian with an elliptical profile, then the reciprocal space response function is also an elliptical Gaussian, for which a single contour is shown in Fig. 4c. The product of such a function with the unperturbed graphite Fourier coefficients is shown in Fig. 4d, in which the coefficients with plus and minus  $k$  character have the same amplitude, but there may be three different amplitudes characteristic of the product of  $F[\rho(\mathbf{r}, E_F)]$  and  $F[b(\mathbf{r})]$ . All real tips will have some asymmetry, and the Fermi surface will be distorted to some extent by the applied bias voltage, so in general one can expect that the actual STM topographs can have Fourier transforms for which all six coefficients are somewhat different from one another. With such a basis of Fourier coefficients, it is possible to reconstruct all the observed atomic resolution STM topographs of graphite [1]. The major extension of this work beyond that of Mizes *et al.*[1] is the understanding of the origin of the Fourier coefficients in  $F[\rho(\mathbf{r}, E_F)]$  and how their relative values depend upon experimental parameters.

Many features of graphite topographs and the STM in general can now be understood at least qualitatively:

1. The 'giant' corrugations[13], which can also be observed in STM topographs collected in constant height mode, and the ease with which graphite yields atomic resolution images are both related to the fact that there is no portion of the Fermi surface at the center of the BZ. Thus, there is no zero wavevector contribution to the STM image from the graphite itself. This means that there is a minimal constant background to mask the oscillations in real-space of the charge density at the Fermi level, and even quite broad tips have little effect on the graphite topograph, since the short wavevector components of the tip are not present in the image. If the tunneling tip is very wide, then the reciprocal-space response function will be correspondingly narrow and will severely attenuate the Fourier coefficients of the image, but the values of  $k$  corresponding to non-zero Fourier coefficients cannot be changed. In effect, graphite electronically sharpens the STM tip; it is not necessary to have a single-atom tip to obtain atomic-resolution topographs.

2. Because of the presence of the Stark field, in general the states that are accessed by the STM are likely not the unperturbed ground state eigenfunctions of the system. This can be a problem in that a particular surface may be characterized by several different topographs as a function of sample bias, clearly complicating the analysis of surface atomic structure. It is also an opportunity to study these perturbed states and the effects of symmetry breaking; in a sense the tip is a controlled defect introduced onto the surface.

3. At low fields, the STM topographs represented by Figs. 1 and 2 are seldom distorted from rotational symmetry; the tip is comparatively far from the surface and the voltage is low, so that only the lowest order moments are important and the field between the tip and surface is essentially cylindrical. Atomic-resolution images that do not have the symmetry of the crystal surface ( e.g. row patterns) are the result of tunneling with an asymmetric tip.

4. The similarity of the images observed on changing the polarity between Figs. 1 and 2 at constant field can be understood by noting that the energy bands of graphite are nearly symmetric in a narrow energy region about  $E_F$  [6-9]. Switching the polarity of the applied bias gives rise to distortions of the ground states that are similar in magnitude but opposite in sign. Since the direction of current flow also changes directions, the overall effect is that the symmetry of the topographs is essentially unchanged. The fact that the magnitude of the corrugations is observed to differ depending on the direction of current flow may be the result of different mobilities for the electrons and holes in graphite.

5. In order to keep the perturbation to the ground state as uniform as possible and thus enable studies of the Fermi surface of a system, STM topographs should be collected in constant height mode. This might more profitably be considered invariant field mode, since the projection of the field onto any plane parallel to the surface is nearly independent of the lateral position of the tip.

For constant current mode, the tip is allowed to move up and down with respect to the surface, and the profile of the field at a given height above the surface will change with lateral position of the tip. Major variations in the mixing of the eigenstates as a function of tip position greatly complicate the interpretation of constant current topographs, since the contours may no longer represent a constant charge density of a single state. Experimentally, good quality atomic resolution topographs of graphite are hard to obtain in constant current mode, typically appearing rather blurred.

6. With a reasonable model of a tip broadening function and a basic understanding of the symmetry of  $F[\rho(r, E_F)]$  and how the coefficients can be perturbed by a localized field, it may be possible to de-convolute  $F[\rho(r, E_F)]$  and  $F[b(r)]$  from a knowledge of their product. Thus, real-space images of both  $\rho(r, E_F)$  and  $b(r)$  can in principle be determined from a single STM current topograph.

The model presented here can be used to explain how all the observed STM topographs of graphite arise and even predict the types of topograph that would be expected for a crystalline surface of any conducting material as long as the details of the Fermi surface are known. Conversely, it appears that STM can be used to investigate the states near  $E_F$  at the surface of a crystal, and thus provide valuable new information about electronic structure, as long as the tip effects are considered correctly. Unfortunately, it does not seem that STM can be used to provide real-space maps of the atomic structures of surfaces without reference to high-quality electronic structure calculations to assist in interpreting the topographs.

This work was supported in part by the US Office of Naval Research, by the National Science Foundation and by the Defense Advanced Research Projects Agency. RSW also received support from the Dreyfus Foundation.

## References

1. H.A. Mizes, S. Park and W.A. Harrison, *Phys. Rev B*, **36** (1987) 4491-4494.
2. G. Binning, H. Fuchs, Ch. Gerber, H. Rohrer, E. Stoll and E. Tosatti, *Europhys. Letts.*, **1** (1986) 31- 36.
3. D. Farrelly, Seeing Quantum Interference Patterns with the Scanning Tunneling Microscope, *Nature* (submitted).
4. I.P. Batra, N. Garcia, H. Rohrer, H. Salemink, E. Stoll and S. Ciraci, *Surf. Sci.*, **181** (1987) 126 - 138.
5. D. Tománek, S.G. Louie, H.J. Mamin, D.W. Abraham, R.E. Thomson, E. Ganz and J. Clarke, *Phys. Rev. B*, **35** (1987) 7790 - 7793.
6. J.W. McClure, *Phys. Rev.* **108** (1957) 612-618; *IBM J. Res. Dev.* **8** (1964) 255-261.
7. J.C. Slonczewski and P.R. Weiss, *Phys. Rev.*, **109** (1958) 272-279.
8. I.L. Spain, in *Chemistry and Physics of Carbon*, (Dekker, New York, 1980), ed. P.L. Walker, Jr., and P. A. Thrower, pp. 1-150.
9. R.C. Tatar and S. Rabii, *Phys. Rev. B*, **25** (1982) 4126-4141.
10. J. Tersoff, *Phys. Rev. Lett.* **57** (1986) 440-443.

11. J. Callaway, *Energy Band Theory* (Academic Press, New York, 1964), pps. 276-283.
12. A. S. Davydov, *Quantum Mechanics* (Pergamon Press, Oxford, 1977), pp. 191-193.
13. J. M. Soler, A. M. Baro, N. Garcia, and H. Rohrer, *Phys Rev. Lett.* **57** (1986) 444-447.

## Figure Captions

Fig. 1 Experimentally obtained STM topographs of the (0001) surface of highly oriented pyrolytic graphite. The average current for all the images was 0.9 nA, and the tip bias with respect to the sample was (a) +22 mV, (b) +25 mV, and (c) +39 mV. The variation in the tip current is shown by both the deflection from horizontal and the color of the scan lines, with the colors black, dark blue, light blue, green, orange and yellow corresponding to increasing current. The topographs do not display true rotational symmetry because the x and y piezoelectric scanners of the STM are not exactly orthogonal. Given that caveat, one can see that the topographs in (a) and (c) are essentially 3-fold rotationally symmetric, whereas that in (b) is 6-fold. The distance scale is shown at the bottom of the figure.

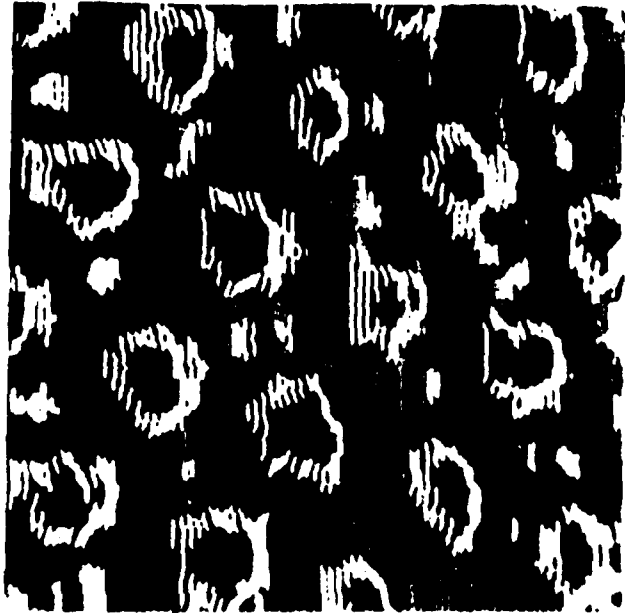
Fig. 2 Experimentally obtained STM topographs of the (0001) surface of highly oriented pyrolytic graphite. The average current for these images was also 0.9 nA, but the tip bias with respect to the sample was (a) -22 mV, (b) -25 mV, and (c) -39 mV. The other comments for Fig. 1 also apply here. The amplitude of the corrugation for the three topographs with negative tip bias was smaller than for positive tip bias, which leads to more distortion of the features and noisier images in this figure than in Fig. 1.

Fig. 3 (a) The real-space crystal structure of graphite, showing the inequivalence of the A and B type atoms, and (b) The Brillouin zone of the graphite lattice, showing the major symmetry lines and points. The Fermi surface is indicated schematically at one of the P lines. The width of the ellipsoids has been exaggerated; the diameter of the actual Fermi surface is about the same as the linewidths in the drawing.

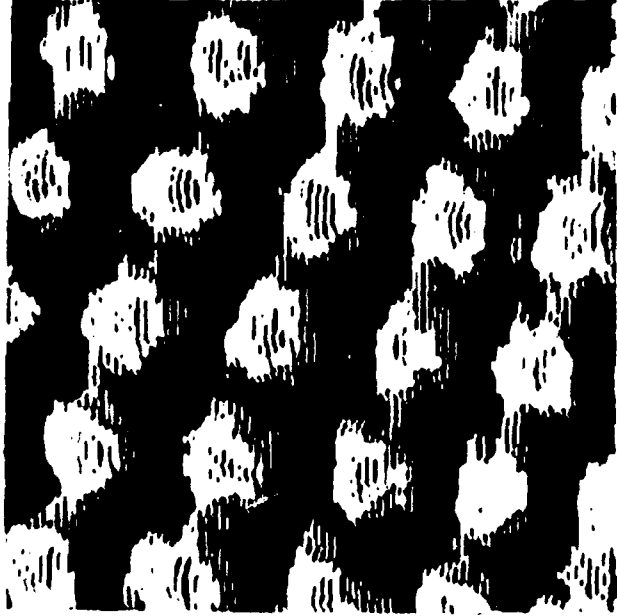
Fig. 4 The surface Brillouin zone of graphite is depicted for different experimental conditions. The Fourier coefficients that contribute to the STM topograph are located at the  $\bar{P}$  points

on the corners of the hexagons, and the intensities of the coefficients are schematically represented by the radii of the filled circles. (a) and (b) illustrate the breaking of the apparent 6-fold symmetry of the coefficients in the presence of a localized field, and (c) and (d) show how the coefficients of the observed image can be affected by an asymmetric tip response function.

(a)



(b)



(c)

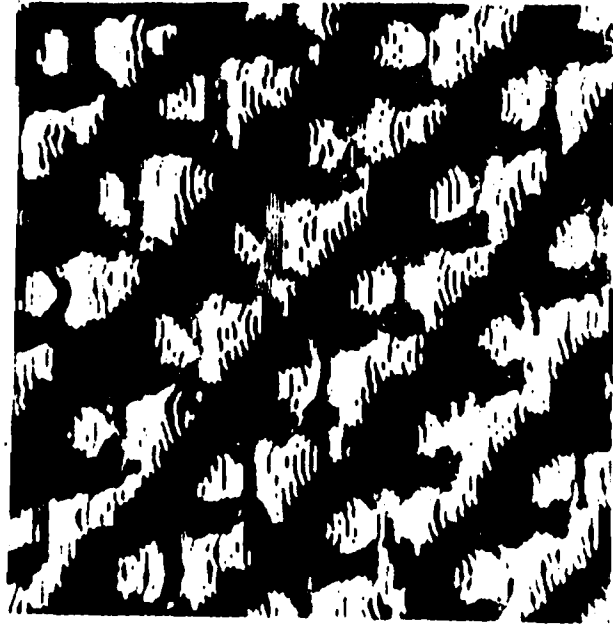


5 Å

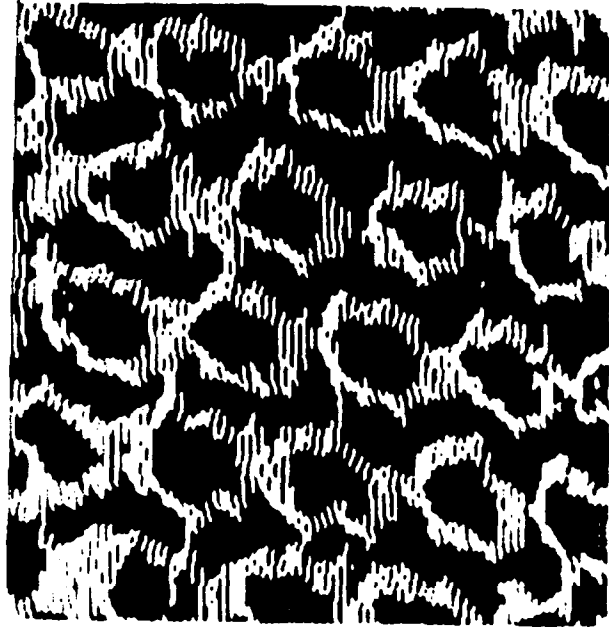
A vertical double-headed arrow is positioned to the right of the text "5 Å", indicating the scale of the micrographs.

**FIGURE 1**

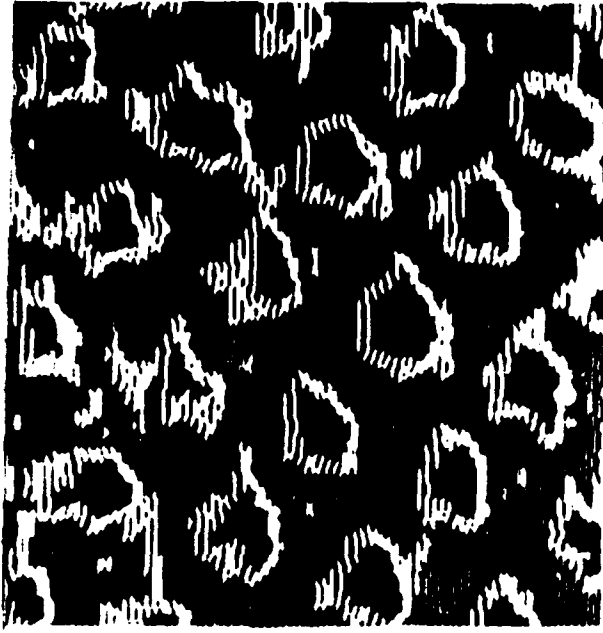
(a)



(b)



(c)



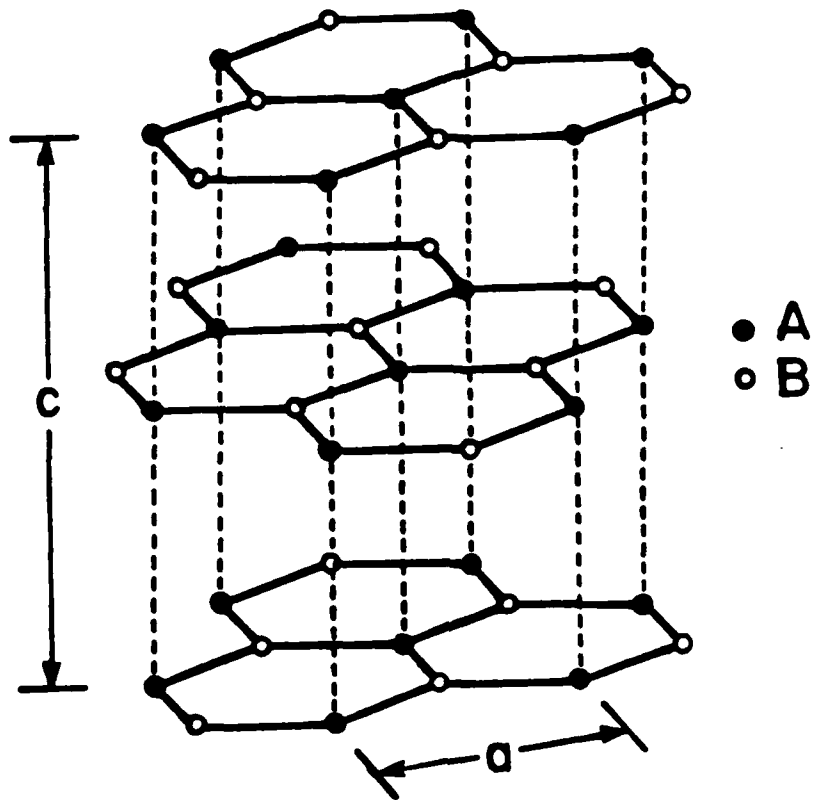
5 Å



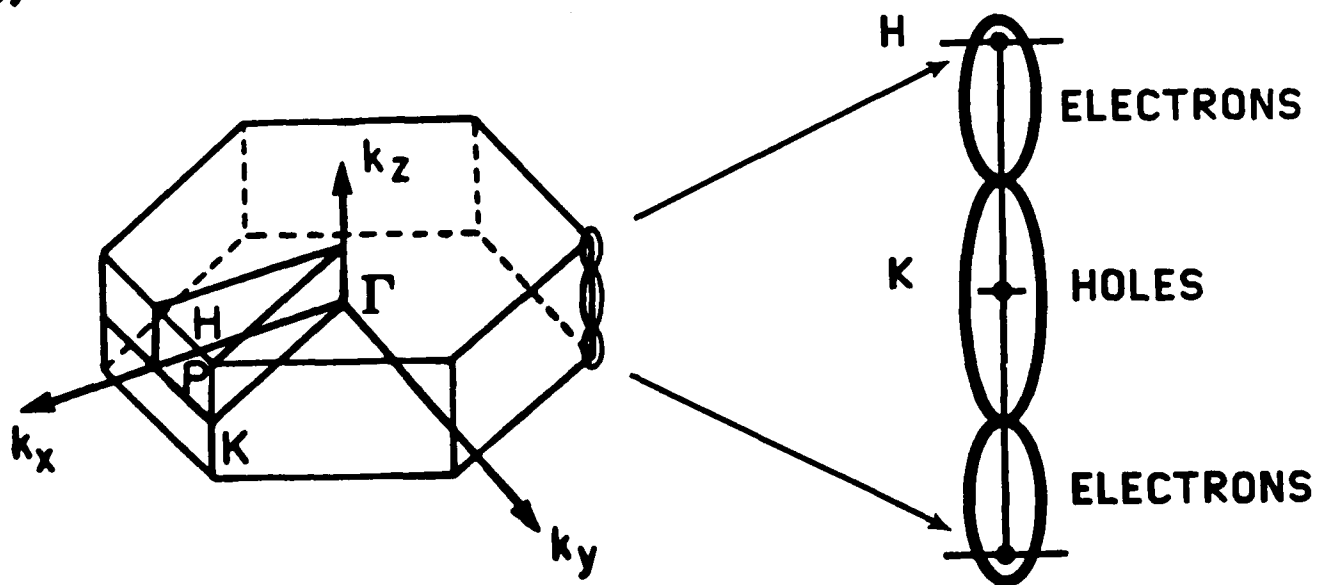
**FIGURE 2**

Fig. 3

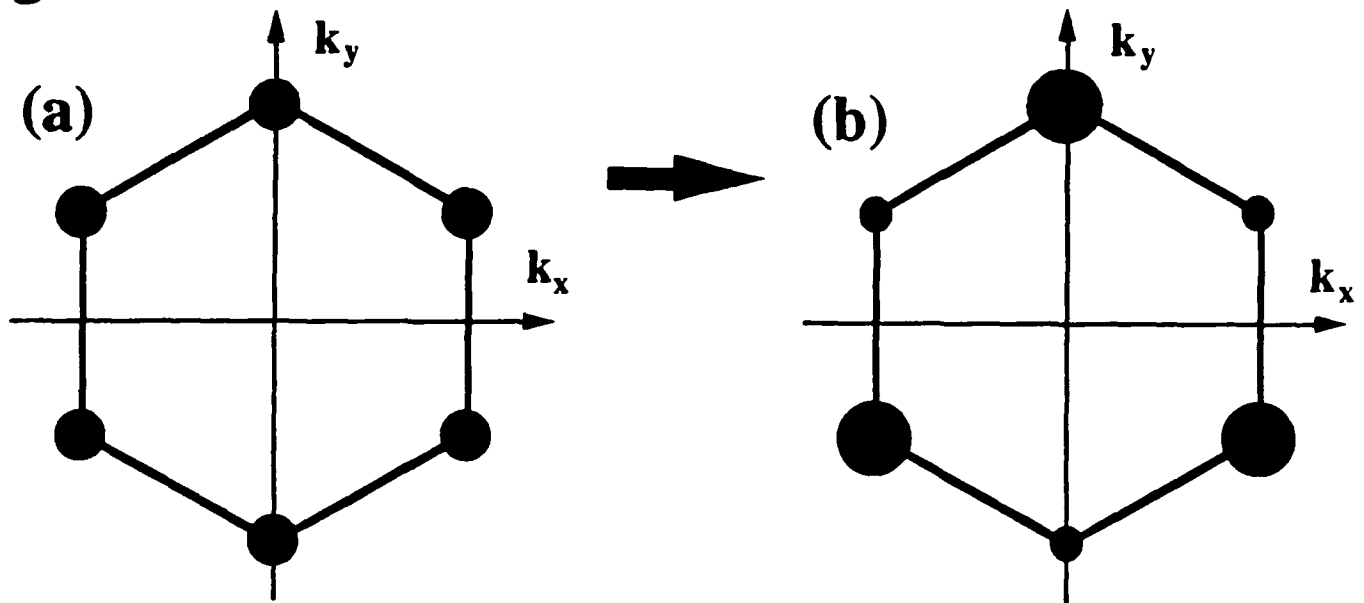
(a)



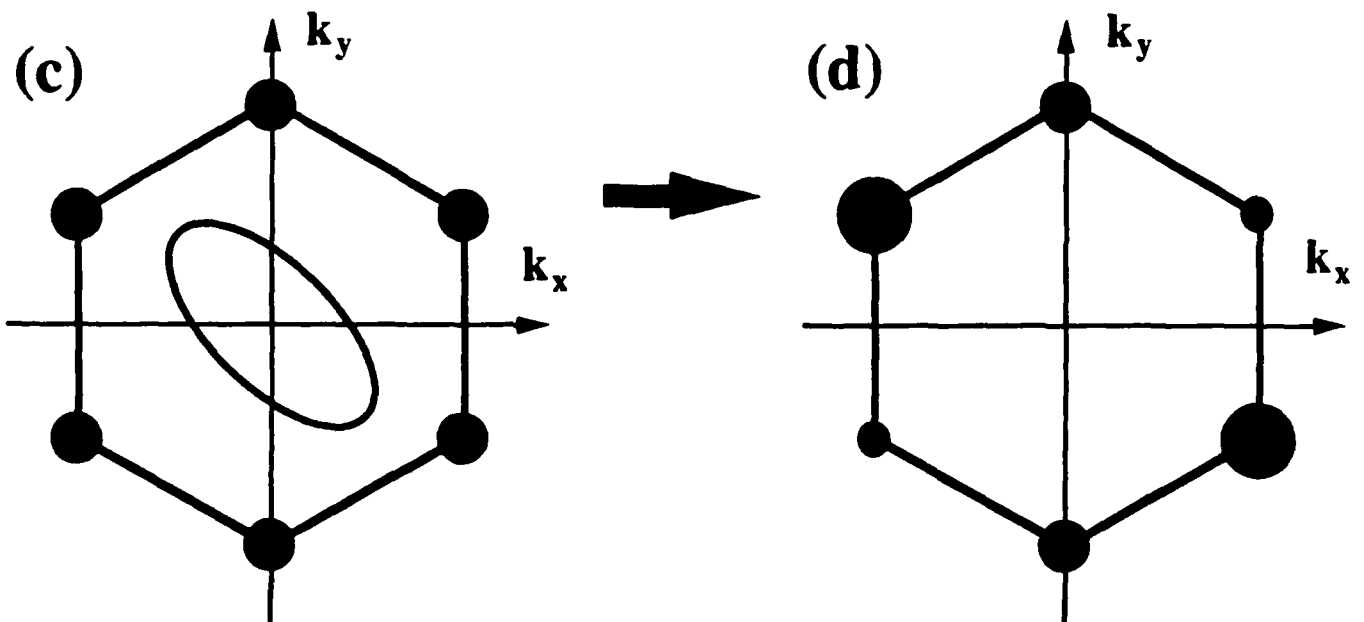
(b)



**Fig. 4**



**Translational Symmetry Breaking by a Cylindrically Symmetric Perturbation**



**Rotational Symmetry Breaking by an Elliptical Tip Response Function**

Dr. J. Babbaschwieler Chemistry & Chem. Engrg. Calif. Inst. of Technology Pasadena, CA 91125	Dr. John Eyster Department of Chemistry University of Florida Gainesville, FL 32611	Dr. Mark Johnson Department of Chemistry Yale University New Haven, CT 06511	Dr. N. Winograd Chemistry Dept. Case Western Res. Univ. University Park, PA 16802	Chief of Naval Research Spec. Assistant, Marine Corps Code 00MC 800 N. Quincy Street Arlington, VA 22217-5000
Dr. Paul G. Barbara Department of Chemistry University of Minnesota Minneapolis, MN 55455-0431	Dr. James F. Garvey Department of Chemistry State University of New York Buffalo, NY 14214	Dr. Sylvia M. Johnson SRI International 333 Ravenswood Avenue Menlo Park, CA 94025	Dr. A. Wold Chemistry Dept. Brown University Providence, RI 02912	Commanding Officer Naval Weapons Support Center Attn: Dr. Bernard E. Douda Crane, IN 47522-5050
Dr. Duncan W. Brown Adv. Technology Mails., Inc. 520-B Daubery Road New Milford, CT 06776	Dr. T.F. George Chemistry/Physics Depts. State University of New York Buffalo, NY 14260	Dr. Z.H. Kafafi Optical Sci. Div., Code 6551 Naval Research Laboratory Washington, DC 20375-5000	Dr. John T. Yates Chemistry Dept. University of Pittsburgh Pittsburgh, PA 15260	Dr. Richard W. Drisko Naval Civil Engineering Lab Code L-52 Port Huenceme, CA 93043
Dr. S. Brechenstein Department of Chemistry State University of NY Buffalo, NY 14214	Dr. Arold Green Quantum Surface Dynamics Br. Naval Weapons Cr.-Code 3817 China Lake, CA 93555	Dr. George H. Morrison Chemistry Dept. Cornell University Ithaca, NY 14853	Dr. E. Yeager Chemistry Dept. Case Western Reserve Univ. Cleveland, OH 41106	Defense Tech. Information Ctr. Building 5 Cameron Station Alexandria, VA 22314
Dr. J. Butler Naval Research Laboratory Code 6115 Washington, DC 20375-5000	Dr. R. Hamers IBM Watson Research Center PO Box 218 Yorktown Heights, NY 10598	Dr. Daniel M. Neumarck Chemistry Department University of California Berkeley, CA 94720	David Taylor Research Center Attn: Dr. Eugene C. Fischer Applied Chemistry Division Annapolis, MD 21402-5067	
Dr. R.P.H. Chang Mats. Science & Engineering Northwestern University Evanston, IL 60208	Dr. Paul K. Hansma Department of Physics University of California Santa Barbara, CA 93106	Dr. H. Tachikawa Chemistry Dept. Jackson State University Jackson, MI 39217	Dr. James S. Munday Chemistry Div., Code 6100 Naval Research Laboratory Washington, DC 20375-5000	
Dr. Paul A. Quarstein Adv. Chem. Technol., Fed. Systems Essman Kodak Company Rochester, NY 14650-2156	Dr. C.B. Harris Chemistry Dept. University of California Berkeley, CA 94720	Dr. W. Unertl Surface Science & Technol. Lab University of Maine Orono, ME 04469	Dr. David Nelson Office of Naval Res. Code 413 800 N. Quincy Street Arlington, VA 22217-5000	
Dr. Richard Colton Code 6170 Naval Research Laboratory Washington, DC 20375-5000	Dr. J.C. Hemminger Chemistry Dept. University of California Irvine, CA 92717	Dr. R.P. Van Duynne Chemistry Dept. Northwestern University Evanston, IL 60201	Dr. Ronald L. Atkins Chemistry Div., Code 385 Naval Weapons Center China Lake, CA 93555-6001	
Dr. J.E. Demuth IBM Watson Research Center PO Box 218 Yorktown Heights, NY 10598	Dr. Rould Hoffmann Chemistry Dept. Cornell University Ithaca, NY 14853	Dr. J.H. Weaver Chemical Engrg & Mats Sci. University of Minnesota Minneapolis, MN 55455	Dr. Bernadette Eichinger Naval Ships Systems Ingr. Station Phila. Naval Base, Code 053 Philadelphia, PA 19112	
Dr. F.J. DiSalvo Department of Chemistry Cornell University Ithaca, NY 14853	Dr. L. Inerrante Chemistry Dept. Rensselaer Polytech. Inst. Troy, NY 12181	Dr. B.R. Weiner Department of Chemistry University of Puerto Rico Rio Piedras, PR 00931	David Taylor Research Station Attn: Dr. H. H. Singerman Code 283 Annapolis, MD 21402-5067	
Dr. A.B. Ellis Department of Chemistry University of Wisconsin Madison, WI 53706	Dr. E.A. Irene Chemistry Dept. Univ. of North Carolina Chapel Hill, NC 27514	Dr. Robert L. Whetten Chemistry Department University of California Los Angeles, CA 90024	Dr. Sachio Yamamoto Naval Ocean Systems Center Code 52 San Diego, CA 91232	
Dr. M.A. El-Sayed Chemistry Department University of California Los Angeles, 90024-1569	Dr. D.E. Irish Department of Chemistry University of Waterloo ONT N2L 3G1, Canada	Dr. R. Stanley Williams Dept. of Chemistry University of California Los Angeles, CA 90024	Carlota Leufroy Office of Naval Research 1030 E. Green Street Pasadena, CA 91106	